This is the peer reviewed version of Dirar, S., Lees, J.M. and Morley, C.T. (2013) Phased Nonlinear Finite Element Analysis of Precracked RC T-Beams Repaired in Shear with CFRP Sheets, *ASCE Journal of Composites for Construction*, Vol. 17, (4). pp. 476–487 which has been published on: http://dx.doi.org/10.1061/(ASCE)CC.1943-5614.0000341

Phased Nonlinear Finite Element Analysis of Precracked RC T-Beams Repaired in Shear with CFRP Sheets

Samir Dirar[1]; Janet M. Lees[2]; and Chris Morley[3]

[1] Lecturer in Structural Engineering, School of Civil Engineering, University of Birmingham, Birmingham, UK, E-mail: s.m.o.h.dirar@bham.ac.uk

[2] Senior Lecturer in Structural Engineering, Department of Engineering, University of Cambridge, Cambridge, UK, E-mail: jmL2@eng.cam.ac.uk

[3] Former Senior Lecturer, Department of Engineering, University of Cambridge, Cambridge, UK, E-mail: ctm1@cam.ac.uk

ABSTRACT

Phased nonlinear finite element (FE) analyses were carried out to predict the behavior of precracked reinforced concrete (RC) T-beams repaired in shear with externally bonded (EB) carbon fiber reinforced polymer (CFRP) sheets and subjected to two loading patterns (LPs). Appropriate constitutive relationships were employed to model the behavior of concrete, internal steel reinforcement, EB CFRP reinforcement, and CFRP-to-concrete interface, and consequently predict the structural behavior and capture the failure modes of the strengthened beams. Three constitutive models for the behavior of concrete in shear were evaluated, namely a total strain rotating crack model and two fixed-angle crack models with either constant or variable shear retention factors.

The majority of published FE studies have considered rectangular sections that were strengthened before testing. The key feature of the FE models presented in this paper is the use of the phased analysis technique to model realistically the process of strengthening RC T-beams under load and predict the structural response of the beams to different loading patterns. Furthermore, the paper provides insight into, and evaluates the accuracy of the three concrete shear models named above. A detailed comparison between the numerical and experimental results included the shear forces at failure, shear force-deflection curves, crack patterns, failure modes, and strains in the internal steel and external CFRP shear reinforcement. The FE models predicted the experimental shear force capacities and crack patterns with sufficient accuracy but underestimated the post-repair stiffness for the beams subjected to Loading Pattern 1 and overestimated the strain in the CFRP sheets.

CE Database subject headings: Concrete beams; Cracking; Fiber reinforced polymers; Finite element method; Reinforced concrete; Retrofitting; Shear Strength; Sheets

INTRODUCTION

Shear failure of reinforced concrete (RC) infrastructure often leads to catastrophic consequences as it occurs in a brittle manner without prior warning. An example of such consequences can be seen in the collapse of the de la Concorde overpass in Laval, Canada which killed or seriously injured eleven people (Johnson et al., 2007).

The need to upgrade or replace a structure that has been identified as having insufficient shear capacity can result in significant user delays as well as high detour and reconstruction costs. Hence, the shear strength enhancement of existing RC infrastructure is of considerable economic and strategic importance, particularly for bridges.

Externally bonded (EB) fiber reinforced polymer (FRP) shear strengthening systems offer several advantages over steel systems, such as high strength-to-weight ratio, corrosion resistance, and ease of application. Thus, EB FRP systems have attracted the attention of many researchers (Khalifa and Nanni 2002; Pellegrino and Modena 2002; Chen and Teng 2003a,b; Deniaud and Cheng 2003; Bousselham and Chaallal 2006) who have confirmed their effectiveness as external shear reinforcement for RC members.

Several design guidelines for the shear strengthening of RC structures with EB FRP reinforcement have been published (*fib* Bulletin 14 2001; The Concrete Society Technical Report No. 55 2012; ACI 440.2R-08 2008). To date, none of these design guidelines has gained wide acceptance. The reason is twofold. First, shear failure of FRP-strengthened RC structures is of notable complexity and depends on many factors that have not yet been considered within a single design model. Second, the majority of the proposed design models employ empirical or semi-empirical expressions for the effective strain in the FRP. This suggests the need for sophisticated models involving compatibility as well as equilibrium considerations in order to address the complex shear behavior of FRP-strengthened RC members.

One possible approach is to use the Finite Element Method (FEM) to predict the behavior and capacity of RC structures repaired in shear with EB FRP reinforcement. The FEM is a powerful analytical tool that can be used to model various combinations of geometry and loading. The nonlinear behavior of FRP-strengthened RC structures can be taken into consideration by incorporating appropriate constitutive laws and iterative procedures. Finite element (FE) analysis, however, carries inherent difficulties in modeling the shear behavior of concrete as well as the behavior of the FRP-to-concrete interface. A careful consideration of these complexities is thus essential to the successful implementation of the FEM in shear strengthening applications.

Many researchers (Wong and Vecchio 2003; Godat et al. 2007; Kim and Vecchio 2008; Chen et al. 2010; Godat et al. 2012) have successfully implemented the FEM to analyze FRP-strengthened RC structures. However, very few researchers (Vecchio and Bucci 1999; Kim and Vecchio 2008) have considered precracked RC structures strengthened in shear with EB FRP reinforcement. Furthermore, FE-based studies modeling the effect of different load histories on the shear behavior of FRP-strengthened RC structures are scarce. This paper addresses FE modeling of precracked RC T-beams strengthened in shear with EB carbon FRP (CFRP) sheets using the commercial FE package DIANA-9.2. The paper presents the predicted structural response of the beams to different load histories, provides insight into three alternative constitutive models for the behavior of concrete in shear, and concentrates in particular on modeling the sequence of loading, unloading, repair and reloading.

RESEARCH SIGNIFICANCE

The majority of existing publications in the field of FE modeling of RC beams strengthened in shear with EB FRP reinforcement (Wong and Vecchio 2003; Chen et al. 2010; Godat et al. 2012) have focused on rectangular sections strengthened before testing. This paper presents FE models for predicting the structural response of shear-critical, CFRP-strengthened RC T-beams to different loading patterns. The FE models presented herein successfully employ the phased analysis technique to model realistically the process of strengthening RC structures under load. Furthermore, this paper provides insight into, and evaluates the accuracy of three widely used constitutive models for the behavior of concrete in shear, namely a total strain rotating crack model and two fixed-angle crack models with either constant or variable shear retention factors (DIANA-9.2 Material Library, 2007).

EXPERIMENTAL INVESTIGATION

The FE models reported in this paper were validated using experimental work carried out by Dirar et al. (2012). They tested five CFRP-strengthened RC T-beams that were precracked before the application of the EB CFRP reinforcement. The experimental parameters considered were load history (precracking the test specimens under two loading patterns), effective beam depth (either 215 mm or 295 mm), and percentage of longitudinal steel reinforcement (either 3.3% or 4.5%). Figure 1 depicts the T-shaped cross-sections considered in the experimental investigation.

The loading regime adopted for testing comprised two loading patterns, each with two loading phases as shown in Figure 2. Phase I included precracking a test specimen under a

load level of 70% of its unstrengthened shear force capacity and then unloading the specimen to 40% of its unstrengthened shear force capacity. Phase II consisted of installing the EB CFRP sheets and loading the specimen up to failure. In Loading Pattern 1 (LP1) the location of the applied load in Phase II was the same as in Phase I, whereas in Loading Pattern 2 (LP2) the loading in Phase II was different to that in Phase I. This enabled a comparison of the mobilization of different shear crack patterns before and after strengthening.

All tested shear spans had 6 mm shear links spaced at 250 mm center-to-center. The external CFRP reinforcement on a tested shear span consisted of three layers of continuous CFRP sheets in the form of a U-wrap around the webs and base of the beam, bonded over a length of shear span of either 1125 mm (F/295/LP1/4.5, F/295/LP2/4.5, and F/295/LP1/3.3) or 820 mm (F/215/LP1/4.6 and F/215/LP2/4.6). The composite material (sheets + adhesive) had a nominal thickness of 1 mm per layer whereas the CFRP sheets had a nominal thickness of 0.131 mm per layer. The CFRP sheets, epoxy resin, and composite material had tensile strengths of 4300 MPa, 30 MPa, and 350 MPa respectively and elastic moduli of 238 GPa, 4.5 GPa, and 28 GPa respectively.

The beams were referenced using the notation F/beam depth (mm)/loading pattern/percentage of longitudinal steel reinforcement. All beams were tested in four-point bending and had a 1000 mm long constant moment region, except that F/295/LP2/4.5 was tested in three-point bending. Additional shear reinforcement was placed in part of F/295/LP2/4.5 thereby leaving a single test span. The base of the web was chamfered in the shear span regions to provide a contoured surface around which the CFRP sheets could be applied. Table 1 details the geometrical and material properties of the tested specimens. The stress-strain curves of the steel reinforcement are depicted in Figure 3. Further details of the experimental program are available in Dirar et al. (2012).

FINITE ELEMENT MODELING STRATEGY

Four of the five CFRP-strengthened beams tested by Dirar et al. (2012) failed in shear due to debonding of the EB CFRP sheets from the concrete. The exception was F/295/LP1/3.3 which failed in flexure. The debonding plane occurred within a thin layer of concrete adjacent to the concrete-to-adhesive interface because the adhesive was stronger than the concrete. Hence, the FRP-to-concrete interface in this study was considered as the adhesive plus the adjacent thin layer of concrete within which debonding occurred. Three-dimensional models incorporating interface elements were deemed necessary to properly simulate the bond-slip behavior at the FRP-to-concrete interface.

The double symmetry of F/295/LP1/4.5, F/295/LP1/3.3, F/215/LP1/4.6, and F/215/LP2/4.6 about the x-y and y-z planes shown in Figure 4(a) enabled a quarter-model to be developed for the nonlinear analysis of these beams. A half-model was developed for F/295/LP2/4.5 since it was symmetric only about the x-y plane shown in Figure 4(b). Appropriate boundary conditions were applied at the plane(s) of symmetry in each case.

DIANA-9.2 Phased Analysis Module (2007) was used to model the different loading phases as well as the staged addition of the CFRP sheets. A phased analysis consists of several calculation phases. The FE model may change between phases by the addition or removal of elements or boundary conditions. In nonlinear phased analysis, the results of the last step in phase *i* are used as initial values for the first step in phase *i*+1. The FE models were subjected to two loading phases. Initially, a FE model was developed with elements representing the concrete, internal steel reinforcement, EB CFRP reinforcement, and FRP-to-concrete interface. However, the elements representing the EB CFRP reinforcement and the FRP-to-concrete interface were set as inactive during Phase I. The remaining FE model consisting of the elements representing the concrete and the internal steel reinforcement was then loaded to 70% and unloaded to 40% of the unstrengthened shear force capacity of the corresponding test specimen. Phase II included activating the elements representing the EB CFRP reinforcement and the FRP-to-concrete interface, and then loading the FE model up to failure. This technique allowed accurate modeling of the physical tests.

GEOMETRICAL MODELING

The following subsections describe briefly the element types used in the FE models. Further information on the chosen elements is available in DIANA-9.2 Element Library (2007).

Concrete and Support Plate

The concrete was modeled with eight-node isoparametric solid brick elements except in the chamfered regions of the web where it was modeled with six-node isoparametric solid wedge elements. These elements were favored because they offered computational efficiency without affecting the accuracy of the model. The brick and wedge elements have three degrees of freedom at each node (translations in the x, y, and z directions shown in Figure 4). The stress field in these elements is three-dimensional and the loading can be in any direction.

Several concrete element sizes were investigated. The failure load predictions obtained by using element sizes of $1.25d_a$ (12.5 mm) and $2.5d_a$ (25mm) differed by approximately 7% (d_a

is the maximum aggregate size) in a few cases whereas the shear force-deflection curves were unaffected. Hence, the 25 mm concrete element size is adopted in this study as it is computationally inexpensive compared to the 12.5 mm element size. This is consistent with both the recommendation of Bažant and Oh (1983) to use element sizes of $3d_a$, and the results of the convergence study carried out by Godat et al. (2012) which showed that the decrease of element sizes from 25 mm to 12.5 mm did not result in significant differences in the numerical results.

The steel support plate was modeled with six-node isoparametric solid wedge elements similar to those used to model the chamfered regions of the beam web.

Steel Reinforcement

All internal steel reinforcement bars were modeled as embedded reinforcement, by rebar (truss-like) elements with no degrees of freedom of their own and strains computed from the displacement fields of the surrounding concrete elements. Ideally, the bond between the concrete and the steel reinforcement should be modeled as a recent study (Chen et al. 2012) reported that a strong bond assumption can either increase or decrease the shear capacity of FRP-strengthened RC beams with increasing number of shear cracks or increasing main shear crack angle respectively. However, other studies (Godat et al. 2007; Kim and Vecchio 2008; Godat et al. 2012) demonstrated that the perfect bond assumption between the concrete and the steel reinforcement can be used successfully to predict the behavior of FRP-strengthened RC structures when bond failure between the two components is not the governing failure mode. Indeed, bond failure between the concrete and the internal steel bars was not the governing failure mode of the tested specimens considered in this study, and so perfect bond was assumed between the concrete and the embedded steel reinforcement.

FRP Reinforcement and FRP-to-Concrete Interface

The unidirectional CFRP sheets were modeled with two-node truss elements spaced at 25 mm center-to-centre along the tested shear spans, with truss elements aligned in the fiber direction (see Figure 4). All truss elements, apart from those next to the support and load positions, had a uniform cross-sectional area equal to the center-to-center distance of the truss elements multiplied by the thickness of the CFRP sheets. The truss elements next to the support and load positions had a uniform cross-sectional area equal to half of the area of the remaining truss elements.

The FRP-to-concrete interface was modeled with eight-node interface elements. These elements connected the edges of the concrete brick and wedge elements to the CFRP truss elements and allowed relative displacements to occur between the two materials.

MATERIAL MODELING

Three different constitutive models for the behavior of concrete in shear were used, namely a constant shear retention model, a variable shear retention model, and a total strain rotating crack model. These models were combined with material models representative of the behavior of concrete in compression and tension, internal steel reinforcement, CFRP sheets, and FRP-to-concrete interface.

Concrete Shear Models

In the fixed-angle crack model, a crack initiates perpendicular to the direction of the principal tensile stress and its direction remains unchanged, i.e. the orientation of the crack is fixed. At the moment of crack formation, there are no shear stresses in the crack plane. With increased loading, the directions of the principal stresses might change. Hence, in the fixed-angle crack model, shear stresses can exist parallel to the existing crack but cannot be fully transferred by the concrete alone due to the presence of a weakened plane. In FE modeling, this is represented by reducing the shear stiffness parallel to the crack using a shear retention factor (β) between zero and unity. Both shear retention models available in DIANA, constant shear retention and variable shear retention, were used in this study.

Bédard and Kotsovos (1986) suggested that shear retention values smaller than 0.1 tend to cause numerical instability whereas shear retention values greater than 0.5 result in high tensile stresses which lead to underestimating the load-carrying capacity of a concrete structure. They also demonstrated that numerical predictions are unaffected significantly by shear retention values between 0.1 and 0.5. Accordingly, two constant shear retention values of 0.1 and 0.2 were initially used. FE predictions (not reported in this paper due to space limitations) of the unstrengthened control beams tested by Dirar et al. (2012) showed that a shear retention value of 0.1 gave more accurate predictions for the peak loads than a value of 0.2. Hence, a shear retention value of 0.1 was adopted in this study.

The variable shear retention model [Eq. (1)] takes into account the deterioration of shear stiffness with opening strain (ε_{cr}) normal to the crack.

$$\beta = \frac{1}{1 + 4447\varepsilon_{cr}} \quad (1)$$

Based on DIANA recommendations, an initial value of β equal to 0.999 was used in order to avoid β becoming equal to unity when the crack arises, i.e., when $\varepsilon_{cr} = 0$.

In the rotating-angle crack model, the crack direction changes with the change in direction of the principal tensile stress. As a result, the crack plane is always a principal plane and shear stresses cannot exist on that plane. Hence, no concrete shear model is required.

Concrete in Compression and Tension

For the models with constant or variable shear retention factors, constitutive relationships based on the theory of plasticity were used to model concrete compression. A compression stress-strain curve developed by Wang et al. (1978) was implemented and Von-Mises yield criterion was used to govern concrete failure in compression. Ideally, a concrete failure criterion should be used. However, the use of von-Mises yield criterion is justified in this study because the experimental behavior of the modeled beams was governed by the tensile and cracking behavior of the concrete whereas the compressive behavior of the concrete played a less important role. For the rotating-angle models, the concrete in compression was modeled by Thorenfeldt's et al. (1987) stress-strain curve which is predefined in DIANA total strain model (DIANA Material Library, 2007). However, Thorenfeldt et al.'s (1987) stress-strain curve becomes comparable to Wang et al.'s (1978) stress-strain curve for f_{cu} = 25 MPa which is a reasonable approximation of the average cube compressive strength of the tested beams.

The behavior of concrete in tension was modeled as linear up to the concrete tensile strength (f_t). A linear tension cut-off criterion governed crack initiation. A crack forms according to the linear tension cut-off criterion if the principal tensile stress exceeds the lesser of f_t and $f_t(1+\sigma_{lateral}/f_{cu})$ where $\sigma_{lateral}$ is the lateral principal stress. The post-cracking behavior of concrete was modeled by a linear tension softening model [Eq. (2)] which relates the ultimate concrete tensile strain ($\varepsilon_{c,ult}$) to the concrete tensile strength, concrete fracture energy (G_f), and crack bandwidth (h_b).

$$\varepsilon_{c,ult} = \frac{2G_f}{h_b f_t} \quad (2)$$

The concrete fracture energy (G_f) was calculated using the formulations of Phillips and Binsheng (1993):

$$G_f = 43.2 + 1.13 f_{cu} \quad (3)$$

In Eq. (3), G_f is given in N/m whereas f_{cu} must be in N/mm^2. Of note is that the fracture energy values predicted by Eq. (3) for the beams considered in this study are practically equal to the fracture energy values that can be calculated using Bažant and Becq-Giraudon's (2002) method.

The crack bandwidth (h_b) is a parameter used to regulate the value of $\varepsilon_{c,ult}$ in order to achieve mesh-independent predictions. It was taken as the cube root of the concrete finite element volume as recommended by DIANA.

The smeared crack approach was implemented where the concrete is treated as a continuum even after cracking.

Crack Unloading and Reloading

Crack unloading and reloading were modeled with a secant approach where the crack normal strain (ε_{cr}) is reversible. Upon crack unloading, the stress normal to crack, crack strain, and crack orientation are stored in order to check for re-opening during a subsequent stage of the loading process. A crack is considered fully closed when $\varepsilon_{cr} = 0$. A closed crack is assumed to re-open if the stress normal to it exceeds the stress which existed upon unloading. Further details can be found in Rots (1988) and DIANA-9.2 Material Library (2007).

Steel Reinforcement and Support Plate

The support plate and the 8 mm, 16 mm, and 20 mm reinforcement bars were modeled as elastic-perfectly plastic materials. However, the 6 mm and 25 mm bars were modeled as materials with plastic hardening according to their experimental stress-strain curves (see Figure 3). The Von-Mises yield criterion was implemented in the plastic region.

FRP Reinforcement and FRP-to-Concrete Interface

The CFRP sheets were modeled as an elastic brittle material. The bilinear bond stress–slip model developed by Lu et al. (2005) represented the behavior of the FRP-to-concrete interface. Lu et al. (2005) and Godat et al. (2012) showed that this model provides accurate

predictions of both the bond strength and the strain distribution in the FRP reinforcement. As depicted in Figure 5, the bond stress-slip relationship is linear up to the peak bond stress (τ_{max}). Debonding initiates if the slip value exceeds s_o, the slip value corresponding to the peak bond stress. The debonding process is modeled by a linear softening function which relates the ultimate slip (s_{max}) to the interfacial fracture energy ($G_{f,int}$). The interfacial fracture energy depends on the width of the FRP sheet (b_f), the width of the concrete specimen bonded to the FRP sheet (b_c) and the concrete tensile strength (f_t). Complete debonding occurs when the slip value exceeds s_{max}.

SOLUTION PROCEDURE

Initially, loads were applied using displacement increments of 0.2 mm but this method encountered convergence difficulties during the unloading-reloading stage. Consequently, this displacement control method was substituted with a load control method where load increments of 1 kN to 2 kN were used. The Quasi-Newton iteration method was used – up to a load level of 80% of the experimental shear force – to achieve equilibrium at the end of each increment. An iteration-based adaptive loading scheme, which decides automatically whether the next step must be an increment or a decrement, was then used up to failure because of its capability to tackle sharp snap-through or softening behavior (DIANA Analysis Manual, 2007). A force norm value of 0.001 was used to specify convergence whereas the force norm value used to specify divergence was 1000. A maximum of 500 iterations were allowed before ending the analysis due to non-convergence. This strategy proved successful as convergence was achieved at every load step. Hence, it was used in all the analyses reported in this paper. Alternatively, it could have been possible to use a dynamic solution procedure (Chen et al. 2011, 2012) or displacement increments in the reloading stage to predict the complete post-peak behavior of the beams. However, the adopted solution strategy was deemed acceptable as the main emphasis was on predicting the structural behavior up to and including peak loads rather than predicting the complete post-peak behavior.

RESULTS AND DISCUSSION

The following subsections compare the FE results with the experimental results. The FE strain and deflection data were collected at the same locations where these parameters were measured experimentally.

Shear Force Capacity

The experimental, V_{exp}, and FE shear forces for the constant, V_{const}, variable, V_{var}, and rotating, V_{rotat}, models at failure are given in Table 2. In general, the FE predictions were in good agreement with the experimental results.

The total strain rotating crack model was the most statistically accurate of the three concrete shear models used in this study. For the majority of the predictions, the model underestimated the shear forces at failure with a mean predicted/experimental ratio of 0.96 and a standard deviation of 0.10. This was to be expected since the rotating crack model assumes that the crack planes are always principal planes and hence underestimates the amount of shear stresses transferred across the cracks. It should be noted that the prediction of the rotating crack model for F/295/LP1/3.3 was not included in calculating the above values due to the erroneous failure mode predicted by the model. This will be further discussed in the next sections.

The fixed-angle crack model with constant shear retention factor overestimated the shear forces at failure for most of the results with a mean predicted/experimental ratio of 1.09 and a standard deviation of 0.09. This result suggests that the constant shear retention value of 0.1 considered in this study is quite reasonable.

The least accurate model was the fixed-angle crack model with variable shear retention factor. The model generally overestimated the shear forces at failure with a mean predicted/experimental ratio of 1.14 and a standard deviation of 0.12. This result suggests that the variable shear retention model in DIANA overestimates the transfer of shear stresses across cracks.

Table 2 shows that the FE models subjected to LP1 had lower shear force capacity than the corresponding FE models subjected to LP2. However, the differences in capacity were about 10% in most of the cases. This result agrees with the experimental results which suggested that differing loading patterns did not generally seem to have a significant effect on the shear force capacity. In beams subjected to LP1, the shear cracks formed prior to strengthening are likely to be mobilized again once strengthened. In beams subjected to LP2, two different sets of shear cracks are stimulated, before and after strengthening. In order to propagate, shear cracks formed after strengthening have to cross the set of flexural cracks formed prior to strengthening. As a result of low stress transfer at the pre-crack interface, a higher load is needed to develop sufficient tensile stress for further crack propagation. This may explain the higher loads attained by the FE models for test specimens subjected to LP2.

Shear Force-Deflection Curves

The experimental and FE shear force-deflection curves are compared in Figure 6. For the purpose of interpreting results, the shear force deflection curves are divided into three stages: loading, unloading, and reloading.

During the initial loading stage, all the FE models predicted the uncracked linear stiffness accurately, suggesting that the elastic constants and boundary conditions were well modeled. The FE models for beams subjected to LP1 correctly predicted the initiation of flexural cracks at a shear force of about 20 kN and thus the predicted shear force-deflection curves turned nonlinear. Between a shear force of 20 kN and 60 kN, flexural cracks extended into the shear spans and turned into inclined cracks resulting in further stiffness deterioration. This was also well predicted by all the FE models for specimens subjected to LP1. Within this shear force range (20 kN – 60 kN), the FE models for beams subjected to LP1 started to overestimate the experimental deflections as can be seen in Figure 6. By the end of the loading stage, the rotating crack models for specimens subjected to LP1 overestimated the experimental deflections by an average of 2.68 mm. The corresponding values for the fixed crack models with constant and nonlinear shear retention factors were 0.88 mm and 0.45 mm respectively. This result demonstrates that both shear retention models accurately predicted the experimental stiffness of the beams subjected to LP1 up to the end of the loading stage. The overestimated deflections predicted by the rotating crack model were to be expected as this model implicitly provides shear softening, or deterioration of concrete shear modulus, at a rate higher than that provided by the fixed angle crack models due to the coaxiality of principal stresses and strains in the rotating crack model (Rots and Blaauwendraad, 1989). This higher shear softening rate resulted in higher deflection predictions by the rotating crack models.

All the FE models accurately predicted the stiffness of the tested beams subjected to LP2 up to the end of the loading stage. This can be explained by the fact that these beams had shorter shear spans during the loading stage (see Figure 2) and thus had fewer cracks compared to the beams subjected to LP1, i.e. the cracked stiffness did not deviate much from the uncracked stiffness.

All the FE models, apart from the rotating crack model for F/215/LP1/4.6, underestimated the deflections at the end of the unloading stage. This is directly influenced by the crack unloading model which assumes linear unloading from any point in the softening branch of the tension softening curve to the origin and therefore underestimates the residual deflections in analyses consisting of loading-unloading cycles. Unloading from a point with high crack

strain (i.e. high x-axis value) to the origin decreases the slope of unloading curve. Hence, for two different points on the softening branch, the unloading model results in a higher unloading rate (greater release of strain for a given reduction of stress) for the lower point than for the upper point. This is why the rotating crack models for beams subjected to LP1, which had higher crack strain compared to the corresponding fixed crack models, experienced higher unloading rates and therefore predicted better the deflections at the end of the unloading stage. As mentioned above, the beams subjected to LP2 did not experience much cracking during the loading stage and therefore their FE predictions were within 0.5 mm of the experimental deflections at the end of the unloading stage.

All the FE models correctly showed higher stiffness at the beginning of the reloading stage due to the activation of the interface and truss elements representing the CFRP strengthening system. Comparing the inclinations of the experimental and predicted reloading parts of the shear force-deflection curves, it can be seen that the FE models slightly underestimated the stiffness of the beams subjected to LP1. It should be noted that the pseudo-stiff response (lower deflections at a given load) shown by some of the fixed crack models subjected to LP1, e.g. the fixed crack models for F/295/LP1/3.3, is a consequence of the underestimated deflections at the end of the unloading stage. For beams subjected to LP2, the FE stiffness predictions reasonably matched the experimental results during the reloading stage.

As can be seen in Figure 6, the shear force-deflection curve predicted by the rotating crack model for F/295/LP1/3.3, which failed in flexure, shows brittle failure characterized by a sudden drop in load. As will be demonstrated below, the crack strain results for a given beam are higher for the rotating crack model than for the fixed crack models. In the case of the rotating crack model for F/295/LP1/3.3, the higher crack strain, which is a measure of crack width, led to the shear capacity falling below the flexural capacity by about 8%. This explains the shear mode of failure predicted by the rotating crack model for F/295/LP1/3.3. The fixed crack models with constant and nonlinear shear retention values correctly predicted the flexural failure of F/295/LP1/3.3 as shown in Figure 6.

Crack Patterns and Failure modes

A significant strength of the FE models presented in this paper is their ability to predict the experimentally observed crack patterns. This can be seen in Figure 7 which illustrates the experimental and typical predicted crack pattern for F/295/LP1/4.5 before applying the CFRP sheets. The vectors shown in Figure 7 represent the normal to the crack strain, which is a measure of crack width. The maximum crack strain of 0.035 shown in Figure 7 was predicted

by the rotating crack model for F/295/LP1/4.5. The corresponding values predicted by the constant and nonlinear shear retention models for the same beam were 0.0081 and 0.0087 respectively. This result further confirms the reason behind the overestimated deflections and underestimated load-carrying capacities predicted by the rotating crack models.

The experimental mode of failure for the tested beams, except F/295/LP1/3.3 which failed in flexure, was characterized by shear failure in the concrete accompanied by the debonding of the CFRP sheets. In order to demonstrate that the FE models can capture the debonding of the CFRP sheets, the interfacial slip profiles at the most critical region (750 mm from the support) of F/295/LP1/4.5 are plotted in Figure 8 for different values of the shear force. The fluctuations from negative to positive values of interfacial slip at a shear force of 66 kN indicate the presence of two inclined cracks at about 125 mm and 200 mm from the soffit of the beam. On further loading to 92 kN, the slip values increased at the vicinity of these cracks. At a shear force of 113 kN, the slip value of 0.2 mm at 125 mm from the beam soffit exceeded the maximum slip value (s_{max}) of 0.17 mm calculated by Lu et al. (2005) model, resulting in the complete debonding of the CFRP sheets. Further interfacial slip results (not reported here due to space limitation) showed that debonding of the CFRP sheets occurred also at the free edge of the sheets close to the loading point and near the beam soffit close to the support. Hence, it could be concluded that the FE models were capable of predicting the debonding mode of failure.

Strain in the shear links and CFRP sheets

The strain results in the shear links and CFRP sheets are presented only for representative beams. Figure 9 shows that the FE models for F/215/LP2/4.6 correctly predicted that initially the strains were negligible and remained so until the formation of inclined cracks. The shear forces at which the links became active were on the whole overestimated. After the links were intersected by the inclined cracks, they exhibited a sharp increase in strain which continued until either yield or failure occurred. The rotating crack model overestimated the strain in the outer and middle shear links at failure. This is mainly because the rotating crack model underestimates the shear stiffness of cracked concrete due to shear softening and consequently overestimates the crack strain as discussed in an earlier section. The fixed crack models provided better predictions of the strain in the outer and middle shear links at failure but generally underestimated the strain at a given load. All the FE models correctly predicted that the inner shear links carried the least amount of strain. This is mainly because the region

close to the load, where the inner links were located, did not experience significant inclined cracking.

The predicted and experimental shear force-strain curves for the CFRP sheets of F/295/LP1/4.5 are presented in Figure 10. The FE models correctly predicted that the CFRP sheets resist the further opening of existing shear cracks and hence start to develop strain with increased loading. However, the strain in the CFRP sheets, and consequently their contribution to the total shear force capacity, was generally overestimated by all the FE models. This result indicates that the bond-slip model overestimated the interfacial shear stresses at a given load. As the shear force capacity for F/295/LP1/4.5 is made up of three components (concrete contribution (V_c), steel contribution (V_s), and CFRP contribution (V_{frp})), all the FE models underestimated the steel and concrete (V_c+V_s) components because all the FE predictions for the shear force capacity of F/295/LP1/4.5 were less than the experimental shear force capacity (see Table 2). The predicted/experimental ratios of both versions of the fixed crack models for the shear force capacity of F/295/LP1/4.5 were 0.99 whereas the rotating crack model provided a predicted/experimental ratio of 0.85 for the same beam. Hence, the rotating crack model unduly underestimated the (V_c+V_s) components. This suggests that the rotating crack model, which generally provided conservative shear force capacity predictions, was artificially better compared to the two versions of the fixed crack model.

Comments on Material Models

The FE analyses modeled the process of strengthening the tested beams under load and reproduced their overall behavior. However, there were some discrepancies between the experimental results and the predictions of the FE models. The effects of the crack unloading model on deflection predictions have been explained in detail in an earlier section. The shear softening incorporated implicitly in the rotating crack model and its effect on deflections and crack strains have also been discussed. The fixed crack models generally underestimated the strain in the shear links at a given load. This was mainly influenced by the overestimated strains in the CFRP sheets which affected the shear force at a given load carried by the links. This result further confirms that the bond-slip model overestimated the transfer on interfacial shear stresses.

SUMMARY AND CONCLUSIONS

This paper presented three-dimensional FE models for precracked RC T-beams repaired in shear with EB CFRP sheets and subjected to different loading patterns. The key features of the FE modeling are the implementation of the phased analysis technique to model realistically the structural response to different loading patterns as well as the staged addition of the CFRP sheets. The predictions of three constitutive models for concrete in shear available in the FE package DIANA-9.2 were compared with experimental results. Based on the results of this study, the following conclusions which relate to the material models used in this study are drawn:

1. The shear force capacity predictions were in good agreement with the experimental results. The mean predicted/experimental capacity ratios achieved by the rotating crack model, the constant shear retention model, and the nonlinear shear retention model were 0.96, 1.09, and 1.14 and the standard deviations were 0.10, 0.09, and 0.12 respectively.
2. The deflection predictions were more accurate for beams subjected to LP2 than for beams subjected to LP1. The deflection predictions for the latter beams were affected by the formulations of both the rotating crack and the crack unloading-reloading models. The rotating crack model, which assumes coaxiality between the principal stresses and strains, underestimated the shear stiffness of cracked concrete and therefore overestimated the deflections at a given load after cracking. The crack unloading-reloading model assumed linear unloading to the origin and therefore underestimated the deflections after the unloading stage.
3. The main experimental mode of failure was characterized by shear failure due to debonding of the CFRP sheets. This mode of failure was well captured by the FE models with slip values in the interface elements indicating the debonding of the CFRP sheets. The fixed crack models correctly predicted the flexural failure of F/295/LP1/3.3 but the rotating crack model predicted a shear mode of failure for this beam due to underestimating its shear force capacity.
4. The FE models overestimated the predicted strains in the CFRP sheets. Consequently, the FE models overestimated the FRP contribution and underestimated the steel and concrete contributions to the shear force capacity. The rotating crack model, which generally provided conservative shear force capacity predictions, was artificially better compared to the fixed crack models with constant and nonlinear shear retention factors.

ACKNOWLEDGMENTS

The financial support of the UK Engineering and Physical Sciences Research Council (EPSRC) through grant GR/S55101/01 is gratefully acknowledged.

REFERENCES

American Concrete Institute (ACI). (2008). “Guide for the design and construction of externally bonded FRP systems for strengthening concrete structures.” *Rep. No. 440 2R-08*, Farmington Hills, Mich.

Bažant, Z. P., and Becq-Giraudon, E. (2002). “Statistical prediction of fracture parameters of concrete and implications for choice of testing standard.” *Cement Concr. Res.*, 32, 529–556.

Bažant, Z. P., and Oh, B. H. (1983). “Crack Band Theory for Fracture of Concrete.” *Matériaux et Constructions*, 16(93), 155–177.

Bédard, C., and Kotsovos, M. D. (1986). “Fracture processes of concrete for NLFEA methods.” *J. Struct. Eng.*, 112(3), 573–587.

Bousselham, A., and Chaallal, O. (2006). “Behaviour of reinforced concrete T-beams strengthened in shear with carbon fiber-reinforced polymer – An experimental study.” *ACI Struct. J.*, 103(3), 339–347.

Chen, G. M., Chen, J. F., and Teng, J. G. (2012). "On the finite element modelling of RC beams shear-strengthened with FRP.” *Constr. Build. Mater.*, 32(1), 13–26.

Chen, G. M., Teng, J. G., and Chen, J. F. (2011). "Finite element modeling of intermediate crack debonding in FRP-plated RC beams." *J. Compos. Constr*., 15(3), 339–353.

Chen, G. M., Teng, J. G., Chen, J. F., and Rosenboom, O. A. (2010). “Interaction between steel stirrups and shear-strengthening FRP strips in RC beams.” *J. Compos. Constr*., 14(5), 498–509.

Chen, J. F., and Teng, J. G. (2003a). “Shear capacity of fiber-reinforced polymer-strengthened reinforced concrete beams: Fiber reinforced polymer rupture.” *J. Struct. Eng.*, 129(5), 615–625.

Chen, J. F., and Teng, J. G. (2003b). “Shear capacity of FRP-strengthened RC beams: FRP debonding.” *Constr. Build. Mater.*, 17(1), 27–41.

Deniaud, C., and Cheng, J. J. R. (2003). “Reinforced concrete T-beams strengthened in shear with fiber reinforced polymer sheets.” *J. Compos. Constr.*, 7(4), 302–310.

DIANA Version 9.2 User’s Manual. (2007). “Analysis Procedures, Part VIII, Phased Analysis.” TNO DIANA BV, Delft, Netherlands, 1st Edition, 375–400.

DIANA Version 9.2 User’s Manual. (2007). “Element Library.” TNO DIANA BV, Delft, Netherlands, 638pp.

DIANA Version 9.2 User’s Manual. (2007). “Material Library.” TNO DIANA BV, Delft, Netherlands, 552pp.

Dirar, S., Lees, J., and Morley, C. (2012). “Precracked reinforced concrete T-beams repaired in shear with bonded carbon fiber-reinforced polymer sheets.” *ACI Struct. J.*, 109(2), 215–224.

fib. (2001). “Externally bonded FRP reinforcement for RC structures.” *TG 9.3*, Int. Federation for Structural Concrete, Lausanne, Switzerland.

Godat, A., Neale, K. W., and Labossière, P. (2007). “Numerical modeling of FRP shear-strengthened reinforced concrete beams.” *J. Compos. Constr.*, 11(6), 640–649.

Godat, A., Labossière, P., Neale, K. W., and Chaallal, O. (2012). “Behavior of RC members strengthened in shear with EB FRP: Assessment of models and FE simulation approaches.” *Comput. Struct.*, 92–93, 269–282.

Johnson, P. M., Couture, A., and Nicolet, R. (2007). “Report of the Commission of inquiry into the collapse of a portion of the de la Concorde overpass.” *Report*, Government of Québec, Canada, 198pp.

Khalifa, A., and Nanni, A. (2002). “Rehabilitation of rectangular simply supported RC beams with shear deficiencies using CFRP composites.” *Constr. Build. Mater.*, 16(3), 135–146.

Kim, S., and Vecchio, F. J. (2008). “Modeling of shear-critical reinforced concrete structures repaired with fiber-reinforced polymer composites.” *J. Struct. Eng.*, 134(8), 1288–1299.

Lu, X. Z., Teng, J. G., Ye, L. P., and Jiang J. J. (2005). “Bond-slip models for FRP sheets/plates bonded to concrete.” *Eng. Struct.*, 27(6), 920–937.

Pellegrino, C., and Modena, C. (2002). “Fiber reinforced polymer shear strengthening of reinforced concrete beams with transverse steel reinforcement.” *J. Compos. Constr.*, 6(2), 104–111.

Phillips, D. V., and Binsheng, Z. (1993). “Direct tension tests on notched and un-notched

plain concrete specimens." *Mag. Concr. Res.*, 45(162), 25–35.

Rots, J. G. (1988). "Computational modeling of concrete fracture." PhD thesis, Delft University of Technology, Delft, The Netherlands.

Rots, J. G., and Blaauwendraad, J. (1989). "Crack models for concrete: discrete or smeared? Fixed, multi-directional or rotating?" *Heron*, 34(1), 56pp.

The Concrete Society. (2012). "Design guidance for strengthening concrete structures using fibre composite materials." *Tech. Rep. No. 55*, Crowthorne, United Kingdom.

Thorenfeldt, E., Tomaszewicz, A., and Jensen, J. J. (1987). "Mechanical properties of high-strength concrete and applications in design." *Proc., Utilization of High Strength Concrete*, Stavanger, Norway, Tapir, Trondheim, 149–159.

Vecchio, F. J., and Bucci, F. (1999). "Analysis of repaired reinforced concrete structures." *J. Struct. Eng.*, 125(6), 644–652.

Wang, P. T., Shah, S. P., and Naaman, A. E. (1978). "Stress-strain curves of normal and lightweight concrete in compression." *ACI Struct. J.*, 75(11), 603–611.

Wong, R. S. Y., and Vecchio, F. J. (2003). "Towards modeling of reinforced concrete members with externally bonded fiber-reinforced polymer composites." *ACI Struct. J.*, 100(1), 47–55.

Table 1 Geometrical and Material Properties of the Tested Specimens

Specimen	Shear span (a), mm	Effective depth (d), mm	Tension steel area (A_s), mm^2	$A_s/b_w d$ (%)	Cube compressive strength (f_{cu}), MPa	Concrete fracture energy (G_f), N/m	Tensile strength, MPa
F/295/LP1/4.5	1125	295	1383	4.5	24	70.3	3.2
F/295/LP2/4.5	1125	295	1383	4.5	27	73.7	2.1
F/215/LP1/4.6	820	215	1030	4.6	32	79.4	3.8
F/215/LP2/4.6	820	215	1030	4.6	25	71.5	4.2
F/295/LP1/3.3	1125	295	1030	3.3	28	74.8	3.6

Table 2 FE and Experimental Shear Forces at Failure

Specimen	V_{exp}, kN	V_{rotat}, kN	V_{rotat}/V_{exp}	V_{var}, kN	V_{var}/V_{exp}	V_{const}, kN	V_{const}/V_{exp}
F/295/LP1/4.5	135	114.8	0.85	134.4	0.99	134.4	0.99
F/295/LP2/4.5	133.5	127.2	0.95	153.6	1.15	142.4	1.07
F/295/LP1/3.3	122.5	113	0.92*	132.2	1.08	132.4	1.08
F/215/LP1/4.6	102.5	96.6	0.94	115.6	1.13	109	1.06
F/215/LP2/4.6	96.5	105	1.09	128	1.33	119.8	1.24
Average			**0.96***		**1.14**		**1.09**
Std. dev.			**0.10***		**0.12**		**0.09**

* The prediction of the rotating crack model for F/295/LP1/3.3 is excluded due to the erroneous failure mode.

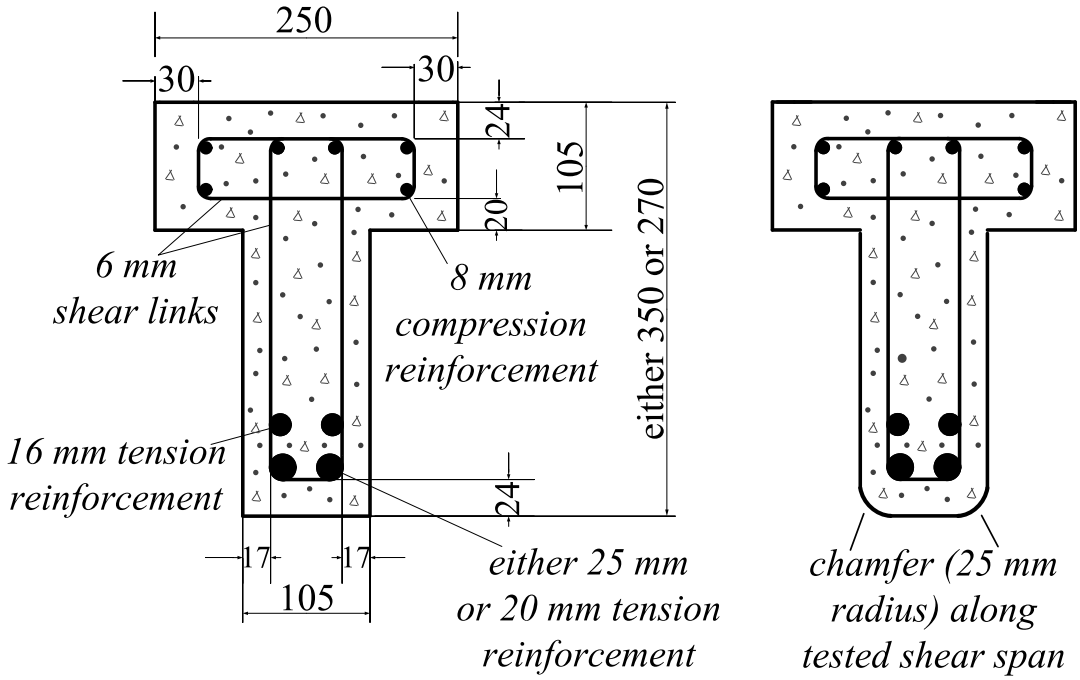

Figure 1 Cross-section details (dimensions in mm)

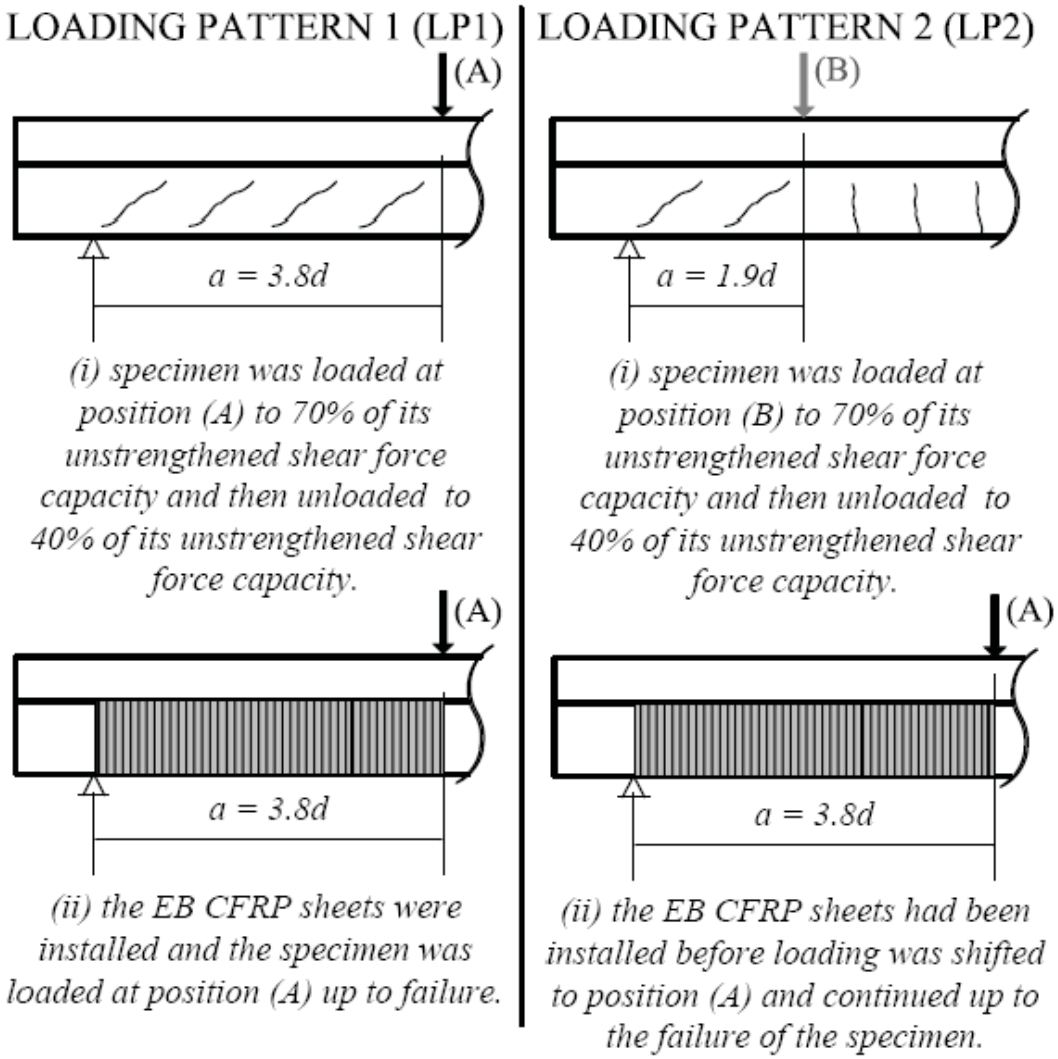

Figure 2 Loading patterns

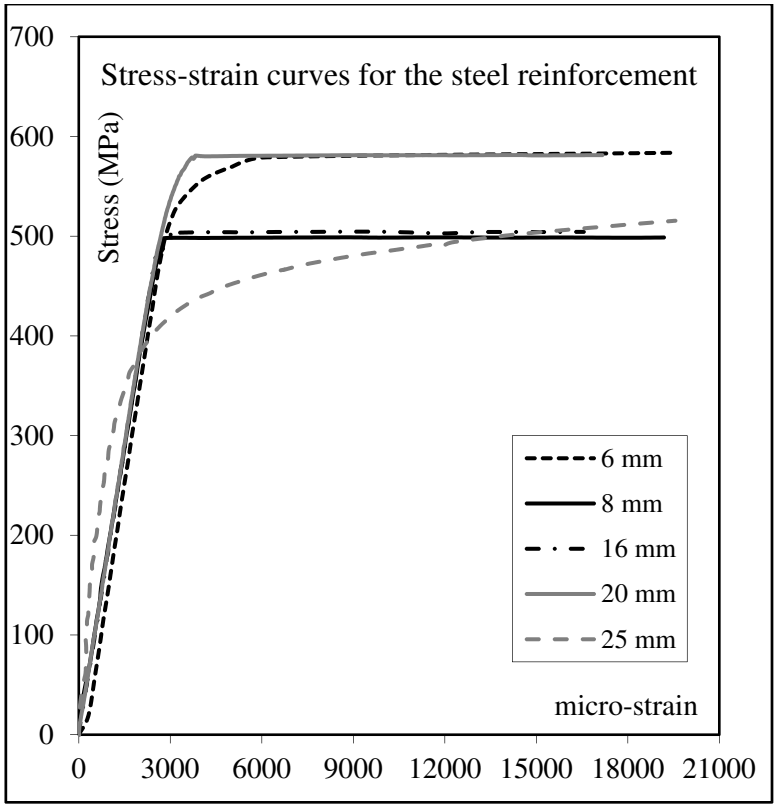

Figure 3 Stress-strain curves for the steel reinforcement

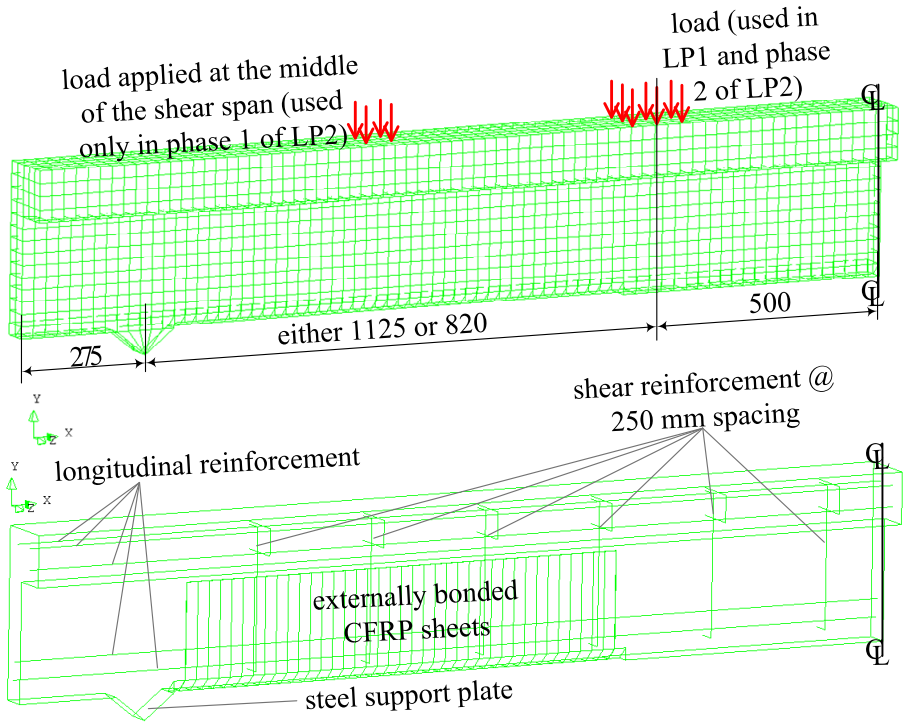

(a) F/295/LP1/4.5, F/295/LP1/3.3, F/215/LP1/4.6, and F/215/LP2/4.6

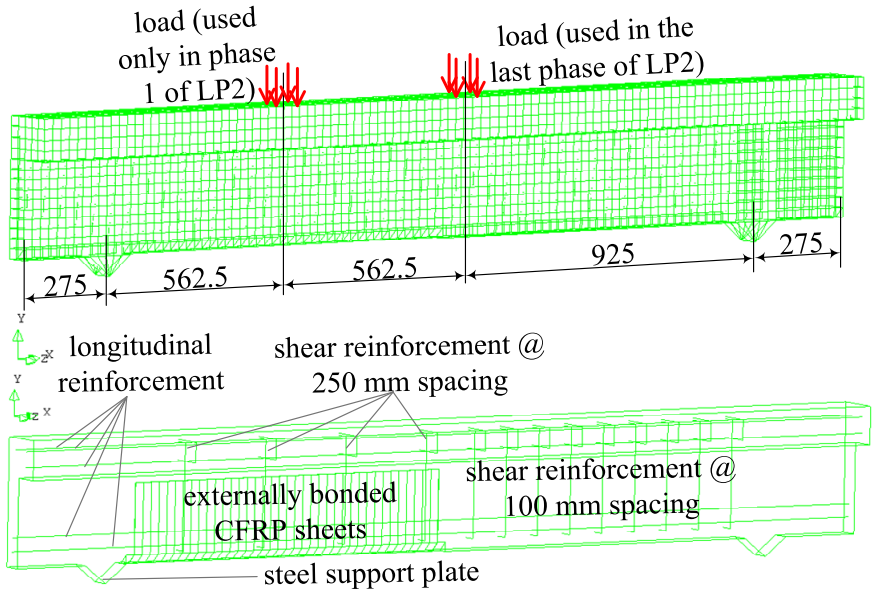

(b) F/295/LP2/4.5

Figure 4 FE models (dimensions in mm); (a) F/295/LP1/4.5, F/295/LP1/3.3, F/215/LP1/4.6, and F/215/LP2/4.6; and (b) F/295/LP2/4.5

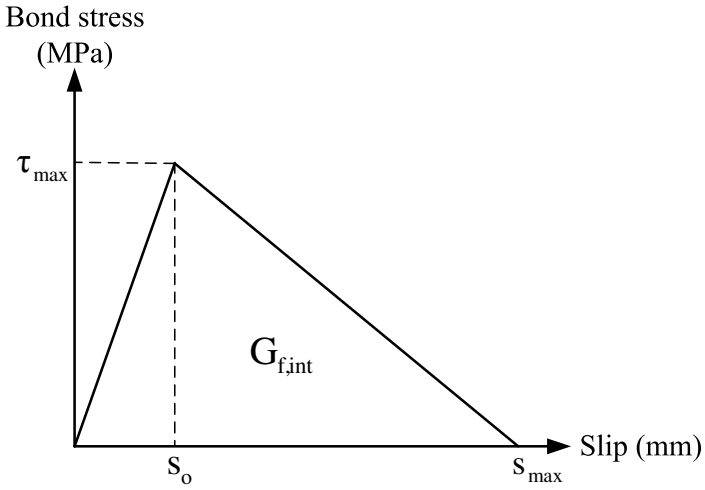

$$\tau = \begin{cases} \tau_{max} \dfrac{s}{s_o} & \text{if } s \le s_o \\ \tau_{max} \dfrac{s_{max} - s}{s_{max} - s_o} & \text{if } s_o < s \le s_{max} \end{cases}$$

$$\beta_w = \sqrt{[2.25\text{-}(b_f/b_c)]/[1.25 + (b_f/b_c)]}$$

$$s_{max} = (2G_{f,int})/(\tau_{max}) \qquad G_{f,int} = 0.308\beta_w^2\sqrt{f_t}$$

$$s_o = 0.0195\beta_w f_t \qquad \tau_{max} = 1.5\beta_w f_t$$

Figure 5 Lu's et al. (2005) bilinear bond-slip model

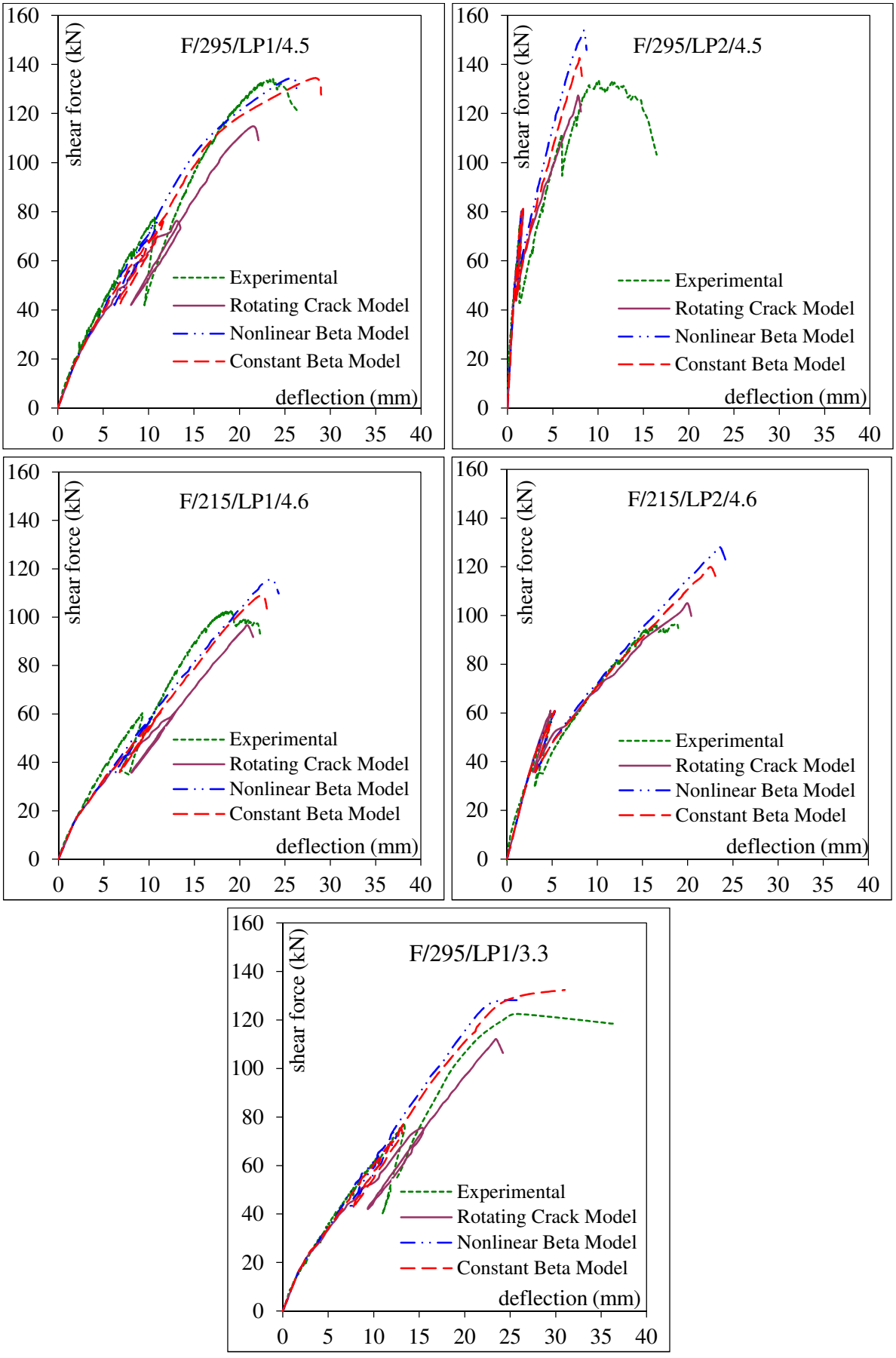

Figure 6 Predicted and experimental shear force-deflection curves

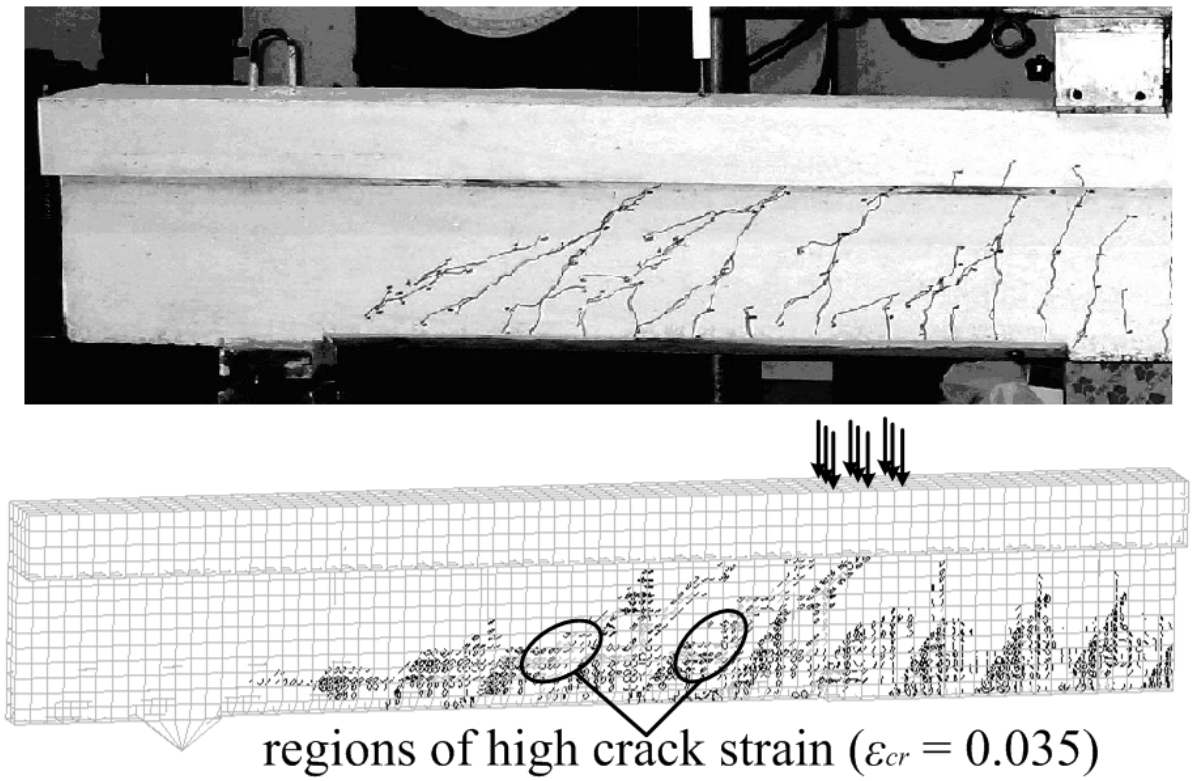

Figure 7 Experimental and typical predicted crack pattern for F/295/LP1/4.5 before strengthening

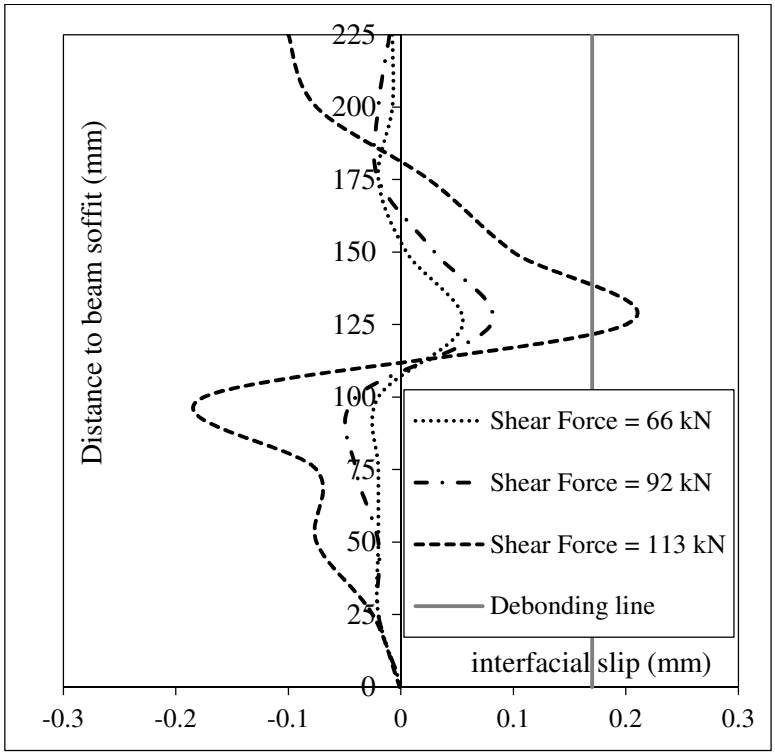

Figure 8 Interfacial slip profiles at 750 mm from the support (rotating crack model for F/295/LP1/4.5)

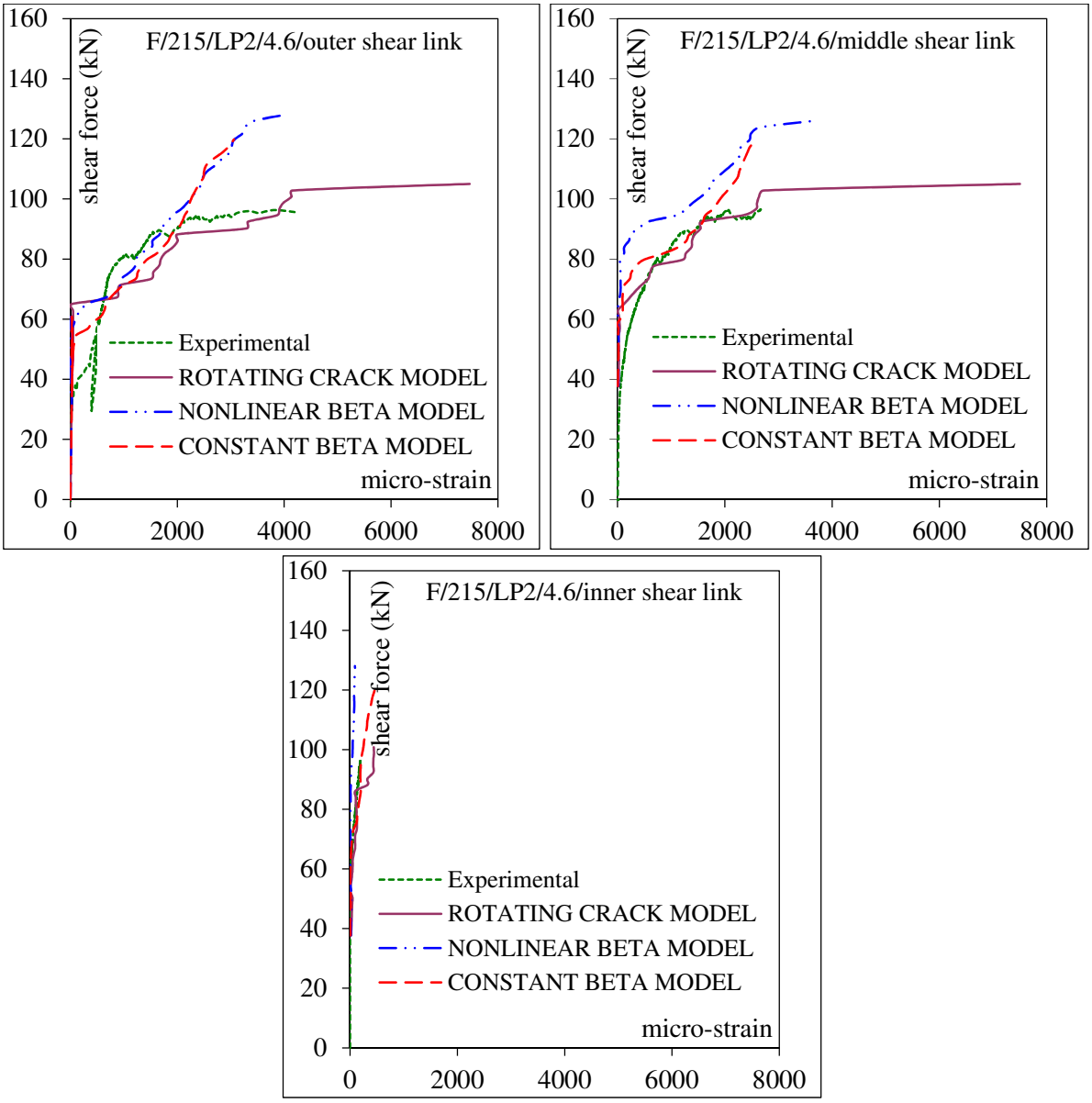

Figure 9 Predicted and experimental strain in the shear links of F/215/LP2/4.6

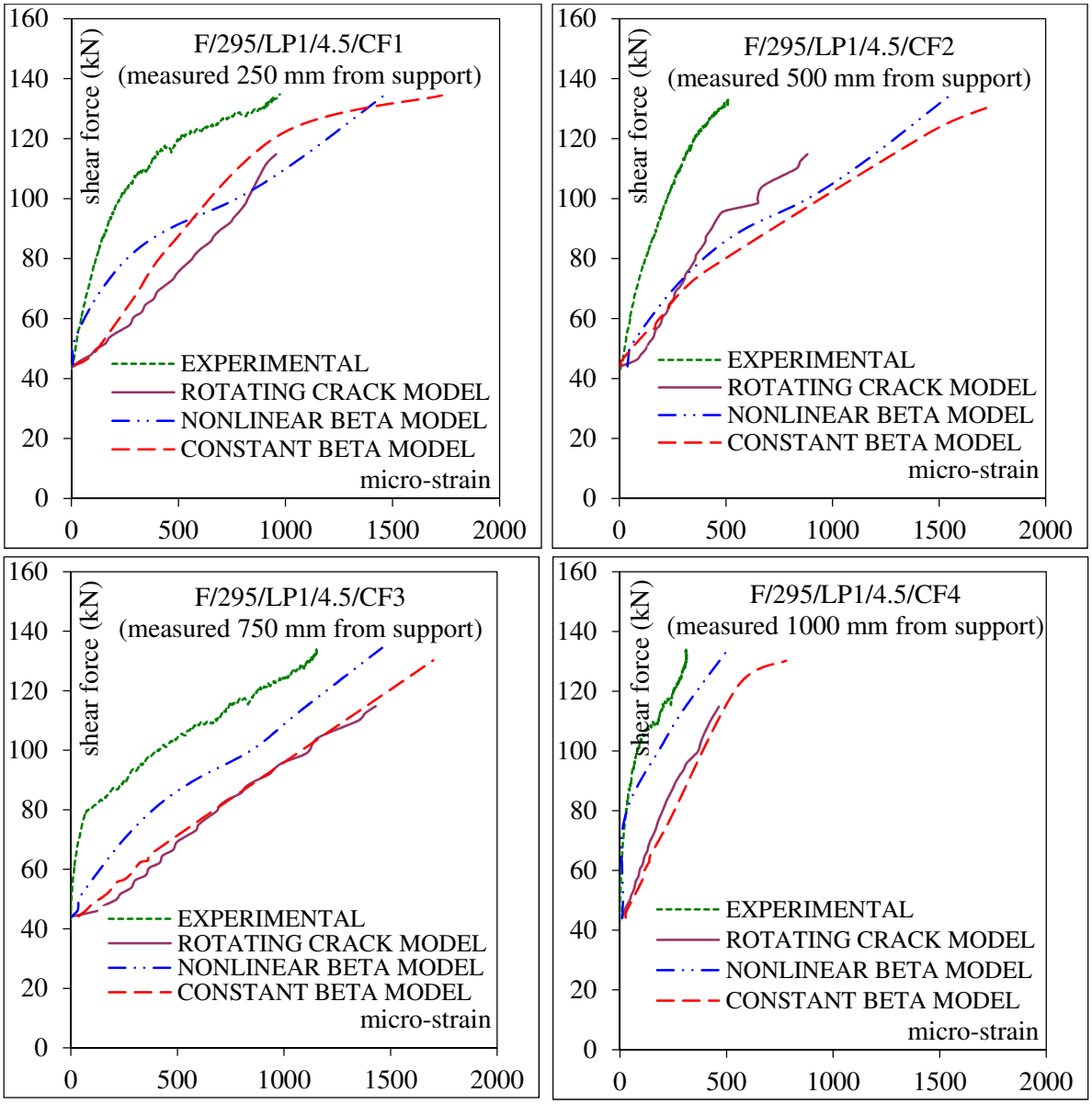

Figure 10 Predicted and experimental strain in the CFRP sheets of F/295/LP1/4.5